

Mobile Transmitters Tracking Using Geodetic Models with Multiple Receivers

Ming-Wang Tu and François Patenaude
Communications Research Centre Canada
3701 Carling Avenue, Box 11490, Station H
Ottawa, ON, Canada, K2H 8S2
Tel: 613-998-9262, 613-990-5878, Fax: 613-990-8842
ming-wang.tu@crc.ca, francois.patenaude@crc.ca

Abstract

The paper presents two geodetic models using data from two or three receivers to track the locations of mobile transmitters.

To apply the techniques in this study, one first has to obtain the estimated angles of arrival (AOAs) and their standard deviations (SDs) from two or three receivers to each transmitter. The histogram-based algorithms in [1] can be used to calculate the estimated AOAs and AOA SDs from a receiver to various transmitters and can be extended for mobile transmitters and fixed receivers with a two/three-receiver (2R/3R) fixing. Once the estimated AOAs and AOA SDs from each receiver to the mobile transmitters are obtained, both of the Spherical and WGS84 geodetic models [2], [3] are used to process the estimated data for each receiver to track the locations of the mobile transmitters with a 2R or 3R fixing. To consider the statistical variations during the location tracking, the concept of confidence ellipse (CE) [4] is applied.

Three sets of simulated data were processed and their results showed significant accuracy for various scenarios. The results of this study demonstrated the effectiveness of using both of the geodetic models to track mobile transmitters with a 2R or 3R fixing.

In general, both of the geodetic models provide a simple and efficient way to track mobile transmitters. The approach is particularly applicable for receivers using fast wideband scanning devices and where items such as AOAs and their instantaneous SDs from several channels are reported per second.

I. Introduction

In mobile communication, the problem of position determination of a mobile transmitter has been studied extensively, particularly in the context of military operations and governmental spectrum licensing. Position estimation can be enhanced by combining geodetic modeling with direction finding (DF) techniques and receivers' global positioning system (GPS) [2] data. In this study, multiple (two and three) receivers were used to perform the DF fixing. Two geodetic models (Spherical and WGS84) were used.

The CRC's Spectrum Explorer [5] can be used as the receiver to scan, collect and pre-process wireless signals. Each scenario may include multiple channels (frequency bands), in or out of regulation. Each channel may have multiple users from various AOAs with different signal-to-noise ratios (SNRs). Each user may use various modulations such as amplitude modulation (AM), frequency modulation (FM), etc. The estimated AOAs and AOA SDs of users for each receiver can be used for the 2R or 3R fixing. With the known GPS coordinates of the receivers and the geodetic models, one can track the mobile transmitters accurately.

Three simulated data sets will be processed using both of the geodetic models for the 2R and 3R fixings. The detailed results will be shown later in this study.

II. Geodetic Models

As described in [2], a point Q on an ellipsoid is determined by $(\phi, \lambda) = (\text{latitude}, \text{longitude})$. The latitude is the angle between the normal at Q and the plane of the Equator. For an ellipsoid, the normal at Q does not go through the center point. The longitude is the angle between the plane of the meridian of Q and the plane of a reference meridian through Greenwich.

In this study, the GPS data include each receiver's coordinates (ϕ, λ) . The AOA is equivalent to the azimuth, defined as the angle with respect to the North Pole in a clockwise direction. Since the earth can be modeled as a sphere or an ellipsoid, the corresponding two models, Spherical and WGS84, were used.

1. Spherical Model

To derive formulas for the transformation of a sphere, two basic laws of spherical trigonometry [3] are used. Referring to the spherical triangle in Fig. 1, with three points having angles (\underline{A} , \underline{B} , \underline{C}) on the sphere, and three great circle angles (\underline{a} , \underline{b} , \underline{c}) connecting them, the Laws of Sines/Cosines declare that

$$\sin \underline{A} / \sin \underline{a} = \sin \underline{B} / \sin \underline{b} = \sin \underline{C} / \sin \underline{c} , \quad (1)$$

$$\cos \underline{c} = \cos \underline{b} \cos \underline{a} + \sin \underline{b} \sin \underline{a} \cos \underline{C} , \quad (2)$$

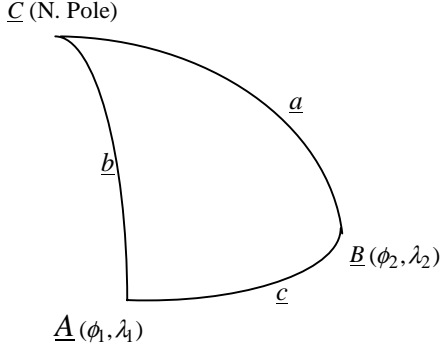


Fig. 1. Spherical triangle

$$\cos \underline{C} = -\cos \underline{B} \cos \underline{A} + \sin \underline{B} \sin \underline{A} \cos \underline{c}. \quad (3)$$

If \underline{C} is placed at the North Pole, it becomes the angle between the two meridians extending to \underline{A} and \underline{B} . If \underline{A} is the starting point on the sphere and \underline{B} the second, \underline{c} is the great circle angle between them, and angle \underline{A} is the azimuth Az east of north which point \underline{B} bears to point \underline{A} . If (ϕ_1, λ_1) and (ϕ_2, λ_2) are for \underline{A} and \underline{B} , respectively, the great arc distance between \underline{A} and \underline{B} is S , and the radius of the earth is $R (=6367.445 \text{ km})$, then

$$\underline{A} = Az, \sin \underline{a} = \cos \phi_2, \sin \underline{b} = \cos \phi_1,$$

$$\sin \underline{C} = \sin(\lambda_2 - \lambda_1), \underline{c} = S/R.$$

Then (1) and (2) become

$$\sin Az / \cos \phi_2 = \sin(\lambda_2 - \lambda_1) / \sin \underline{c}, \quad (4)$$

$$\cos \underline{c} = \sin \phi_1 \sin \phi_2 + \cos \phi_1 \cos \phi_2 \cos(\lambda_2 - \lambda_1). \quad (5)$$

From (4), one can get

$$\cos Az = [\cos \phi_1 \sin \phi_2 - \sin \phi_1 \cos \phi_2 \cos(\lambda_2 - \lambda_1)] / \sin \underline{c}. \quad (6)$$

From (5) and (6), one can get

$$\phi_2 = \arcsin(\sin \phi_1 \cos \underline{c} + \cos \phi_1 \sin \underline{c} \cos Az). \quad (7)$$

Given (ϕ_1, λ_1) and (ϕ_2, λ_2) for receivers 1 and 2 (R1 and R2), (5) can be used to find the S (D12) between R1 and R2. Then the corresponding Az (A12, A21) between R1 and R2 can be found by using (4) and (6). For transmitter 1 (T1) with AOA1 from R1 and AOA2 from R2, by properly subtracting (A12, A21) from (AOA1, AOA2), one can find the two internal angles at the R1 and R2 corners of the R1-R2-T1 triangle. Then the internal angle at the T1 corner can be calculated by using (3). The D13 between R1 and T1 can then be calculated by using (1). Then the problem with given D13 and AOA1 from R1 is next. (5) and (7) can be used to find the (ϕ_3, λ_3) which is the location of T1. The same procedure can be repeated for multiple AOA1 and AOA2 sets for various mobile transmitters. The above 2R fixing procedure can be extended to a 3R fixing by processing two receivers at a time.

2. WGS84 Model

The following mid-latitude formulas [2] (8), (9) and (10) can be used to find the arc distance S and the two azimuths between known points at (ϕ_1, λ_1) and (ϕ_2, λ_2) :

$$S \sin Az = Nl \cos \phi [1 - (l \sin \phi)^2 / 24 + (1 + \eta^2 - 9\eta^2 t^2) b^2 / 24V^4], \quad (8)$$

$$S \cos Az = Nb' \cos(l/2) [1 + (1 - 2\eta^2)(l \cos \phi)^2 / 24 + \eta^2(1 - t^2)b^2 / 8V^4], \quad (9)$$

$$\Delta Az = l \sin \phi [1 + (1 + \eta^2)(l \cos \phi)^2 / 12 + (3 + 8\eta^2)b^2 / 24V^4], \quad (10)$$

where

$$\phi = (\phi_1 + \phi_2) / 2, l = \lambda_2 - \lambda_1, b = \phi_2 - \phi_1, t = \tan \phi, \eta = e' \cos \phi,$$

$$e'^2 = (a^2 - b^2) / b^2, V^2 = 1 + \eta^2, f = (a - b) / a, c = a^2 / b,$$

$$N = a / \sqrt{1 - f(2 - f) \sin^2 \phi}, V = c / N, b' = b / V^2,$$

and a ($=6378.137 \text{ km}$) is the semimajor axis (equatorial radius) of earth; b is the semiminor axis (polar radius) of earth; f ($=1/298.257223563$) is the flattening; e' is the second eccentricity and c is the radius of curvature.

(10), (11) and (12) can be used iteratively to find the (ϕ_2, λ_2) at a given S and azimuth Az east of north from (ϕ_1, λ_1) :

$$l = S \sin Az [1 + (l \sin \phi)^2 / 24 - (1 + \eta^2 - 9\eta^2 t^2) b^2 / 24V^4] / N \cos \phi, \quad (11)$$

$$b' = S \cos Az [1 - (1 - 2\eta^2)(l \cos \phi)^2 / 24 - \eta^2(1 - t^2)b^2 / 8V^4] / N \cos(l/2). \quad (12)$$

Note that the S between the estimated location of a transmitter and a known receiver in WGS84 model can be estimated by using (4) and (5) in the Spherical model (note the $\underline{c} = S/R$) combined with the averaged spherical-to-ellipsoidal correction factor. From [3], the ratio for the length of a radian of latitude along a meridian on the sphere to that on the ellipsoid is

$$C_m(\phi) = R(1 - e^2 \sin^2 \phi)^{3/2} / [a(1 - e^2)], \quad (13)$$

and the ratio for the length of a radian of longitude along a parallel on the sphere to that on the ellipsoid is

$$C_p(\phi) = R(1 - e^2 \sin^2 \phi)^{1/2} / a, \quad (14)$$

where $e = (1 - b^2/a^2)^{1/2}$ is the eccentricity of the ellipsoid. Given (ϕ_1, λ_1) and (ϕ_2, λ_2) , the averaged spherical-to-ellipsoidal correction factor is

$$C_{sp_ellips} = \left[\sqrt{C_m^2(\phi_1) + C_p^2(\phi_1)} + \sqrt{C_m^2(\phi_2) + C_p^2(\phi_2)} \right] / 2. \quad (15)$$

The relationship between the S in WGS84 model (S_{WGS84}) and the S in Spherical model (S_{sp}) is

$$S_{WGS84} = S_{sp} / C_{sp_ellips}. \quad (16)$$

Given (ϕ_1, λ_1) and (ϕ_2, λ_2) for R1 and R2, (8) and (9) can be used to find the S (D12_WGS84) between R1 and R2. Then the corresponding A_z (A12, A21) between R1 and R2 can be found by using (8), (9) and (10). Again, for T1 with AOA1 from R1 and AOA2 from R2, by properly subtracting (A12, A21) from (AOA1, AOA2), one can find the two internal angles at the R1 and R2 corners of the R1-R2-T1 triangle. Then the internal angle at the T1 corner can be calculated by using (3). Note that since the Spherical model equation (3) is used in the WGS84 model, (15) has to be used. That is, D12_WGS84 should be multiplied by (15) to get the D12_Spherical, which can be then used to find the internal angle at the T1 corner. The D13_Spherical between R1 and T1 can then be calculated by using (1). Then the D13_Spherical should be divided by (15) to get the D13_WGS84. Then the problem with given D13_WGS84 and AOA1 from R1 is next. (10), (11) and (12) can be used to find the (ϕ_3, λ_3) which is the location of T1. Again, the same procedure can be repeated for multiple AOA1 and AOA2 sets for various mobile transmitters. The above 2R fixing procedure can be extended to a 3R fixing by processing two receivers at a time.

III. 2R/3R Fixing and Confidence Ellipse (CE)

Both of the 2R and 3R fixings were investigated in this study. The concept of CE was also applied.

1. 2R Fixing

The detailed calculation procedure for the 2R fixing has been described in both the Spherical and WGS84 model sections. One can repeat the procedure for multiple AOA1 and AOA2 sets for various mobile transmitters to track those mobile transmitters.

2. 3R Fixing

In Fig. 2, K, L and M represent the receivers and A, B, C the corresponding corners of a triangle. From [4], the best estimated location of the transmitter is at V , the meeting-point of lines AT and BU , where

$$\frac{BT}{TC} = \frac{D_M^2 \sigma_{\psi M}^2 \sin^2 BCA}{D_L^2 \sigma_{\psi L}^2 \sin^2 ABC}, \quad (17)$$

$$\frac{CU}{UA} = \frac{D_K^2 \sigma_{\psi K}^2 \sin^2 CAB}{D_M^2 \sigma_{\psi M}^2 \sin^2 BCA}, \quad (18)$$

where $D_K = KC, D_L = LA, D_M = MB$ and $\sigma_{\psi J}$ is the AOA SD from receiver J ($=K, L, M$). By Menelaus' Theorem [6],

$$CA \times VU \times BT = UA \times BV \times TC, \text{ thus}$$

$$\frac{BV}{VU} = \frac{BT}{TC} \times \frac{CA}{UA} = \frac{BT}{TC} \times \left(1 + \frac{CU}{UA}\right). \quad (19)$$

The detailed calculation procedure for the 2R fixing has been described in both the Spherical and WGS84 model sections. For various mobile transmitters, one can repeat the 2R fixing procedure for multiple AOA1, AOA2 and AOA3 sets for the 3R fixing to find the sets of (A, B, C) . Once the sets of (A, B, C) are found, one can use (17), (18) and (19) to find the V s to track those mobile transmitters.

3. Confidence Ellipse

The CE with probability P is the probability that the V of a mobile transmitter will lie within the area bounded by an elliptical contour with semimajor axis r and semiminor axis s . The related equations [4] are defined as follows:

$$\frac{X^2}{r^2} + \frac{Y^2}{s^2} = -2 \log_e(1 - P), \quad (20)$$

where

$$\frac{1}{r^2} = 2\kappa - \nu \tan \varphi, \quad \frac{1}{s^2} = 2\mu + \nu \tan \varphi, \quad \kappa = \sum_J \frac{\sin^2 \theta_J}{\sigma_{\psi J}^2 D_J^2},$$

$$\mu = \sum_J \frac{\cos^2 \theta_J}{\sigma_{\psi J}^2 D_J^2}, \quad \nu = \sum_J \frac{\sin \theta_J \cos \theta_J}{\sigma_{\psi J}^2 D_J^2}, \quad \tan 2\varphi = -\frac{2\nu}{\kappa - \mu},$$

and θ_J is the AOA from receiver J . Note that X and Y rotate through an angle φ relative to the coordinates x and y . Also the $(r, s, \kappa, \mu, \nu, \varphi)$ and the CE vary as the AOA varies. The CE can be applied to both of the 2R and 3R fixings.

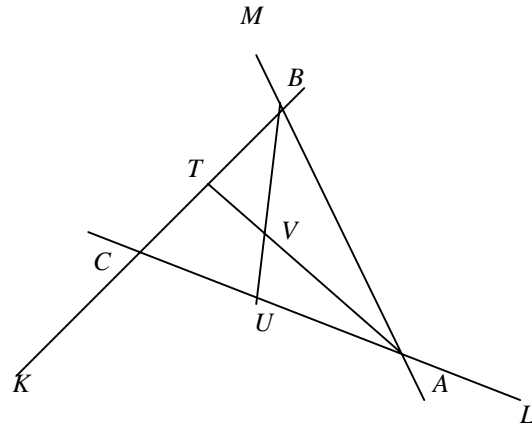


Fig. 2. 3R Fixing

IV. Simulated Results

Three receivers located at Mont Royal (R1) and St-Remi (R2) in Quebec, Canada and a dummy location (R3) were simulated with (ϕ, λ) equal to $(45.50^\circ, -72.39^\circ)$, $(45.28^\circ, -72.33^\circ)$ and $(45.43^\circ, -72.68^\circ)$, respectively. For the Spherical model, the arc distance R1_R2 (D12) = 25.207 km, R2_R3 (D23) = 31.979 km and R3_R1 (D31) = 23.893 km. For the WGS84 model, D12 = 25.211 km, D23 = 32.058 km and D31 = 23.965 km. One and two transmitters with estimated 25-dB SNR were also simulated. In this study, $AOAi_Tj$ represents the true azimuth from receiver i to transmitter j . For the case of one motionless transmitter, the $AOAi_T1$ set was used, while T1&T2 sets with two indices ($AOAi_T1\&2(1,2)$) were used for the case of two mobile transmitters.

From [1], the AOA SDs among various single-receiver scenarios with 25-dB SNR are around 2° . Thus, to simulate multi-receiver scenarios with a 25-dB SNR, normal distributions with 1° and 2° SD were used with various seeds for each snapshot as the signal model of the AOA SDs of the transmitters from each receiver. A snapshot refers to multiple wideband scans of data that are averaged to produce estimates of the AOAs and AOA SDs. Note that the estimated AOAs and AOA SDs in [1] for a single-receiver scenario can be used as the inputs from each receiver in this study. Certainly, the estimated AOAs and AOA SDs from each receiver to the transmitters can be obtained by methods other than [1].

For the 2R fixing, (R1, R2) and (AOA1, AOA2) were used. For the 3R fixing, (R1, R2, R3) and (AOA1, AOA2, AOA3) were used. In this study, 20 snapshots of simulated data were generated for each case using the sets of the $AOAi_Tj$ with an AOA SD for transmitter j from receiver i . Among the 20 snapshots, (r_max, s_max) were calculated by finding the maximum of (rs, ss) , and the corresponding CE (represented by an ellipse) was calculated for each case. In related figures, the $(r_max, s_max)_Tj$ of the CE was displayed in km. $Vavg_Tj$, the center of a CE in (latitude_degree, longitude_degree), was calculated by averaging V_Tjs among 20 snapshots. The true location of Tj (True_ Tj in (latitude_degree, longitude_degree)) was calculated by using zero AOA SDs and was represented by a star.

For each scenario, both of the Spherical and WGS84 models were used and the recalculated $AOAi_Tj$ (Rec_ $AOAi_Tj$, azimuth from Ri to $Vavg_Tj$) was calculated. The $AOAi_Tj$ error ($Er_AOAi_Tj = Rec_AOAi_Tj - AOAi_Tj$) was calculated in degree to check the accuracy. The root-mean-square distance (RMSD_ Tj in km) between V_Tjs and the True_ Tj among 20 snapshots was calculated. The corresponding

area of each CE (AREACE_ Tj in km^2) was also calculated. For the cases of mobile transmitters, $Er_AOAi_Tj(1,2)$, True_ $Tj(1,2)$, $Vavg_Tj(1,2)$, $(r_max, s_max)_Tj(1,2)$, RMSD_ $Tj(1,2)$ and AREACE_ $Tj(1,2)$ were calculated.

Simulated Test1 Scenario: Motionless T1 for a 2R fixing, (AOA1, AOA2) = $(225^\circ, 315^\circ)$ with (I): 1° AOA SD and $P = 50\%$ CE; (II): 1° AOA SD and $P = 99\%$ CE; (III): 2° AOA SD and $P = 99\%$ CE. For the Spherical and WGS84 models, among 20 snapshots, the results of (I) are shown in Fig. 3 and Fig. 4, respectively. The results of (II) are shown in Fig. 5 and Fig. 6, respectively. The results of (III) are shown in Fig. 7 and Fig. 8, respectively. The related results are shown in TABLE I.

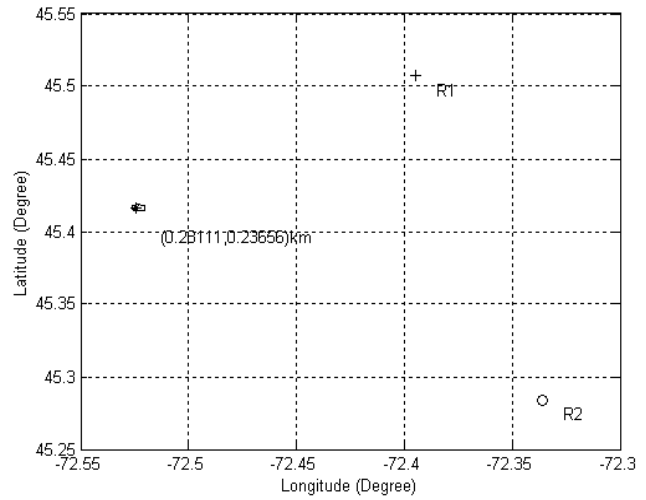


Fig. 3. Test1, Spherical, 1° SD, 50% CE, Avg_20snaps

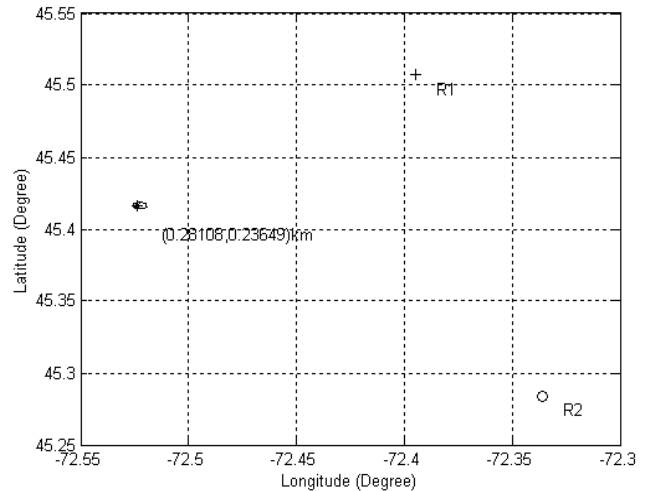


Fig. 4. Test1, WGS84, 1° SD, 50% CE, Avg_20snaps

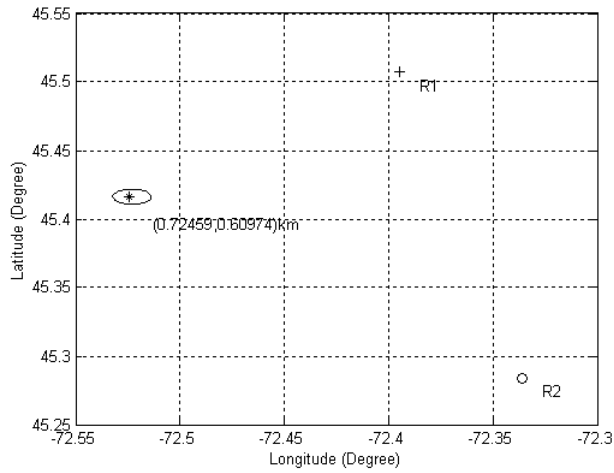


Fig. 5. Test1, Spherical, 1° SD, 99% CE, Avg_20snaps

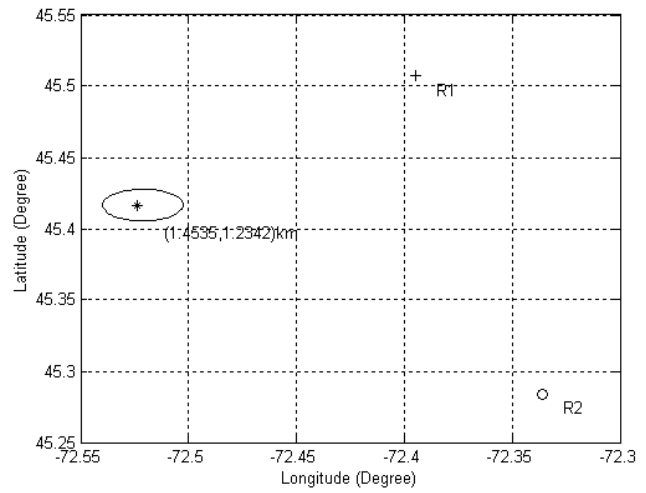


Fig. 8. Test1, WGS84, 2° SD, 99% CE, Avg_20snaps

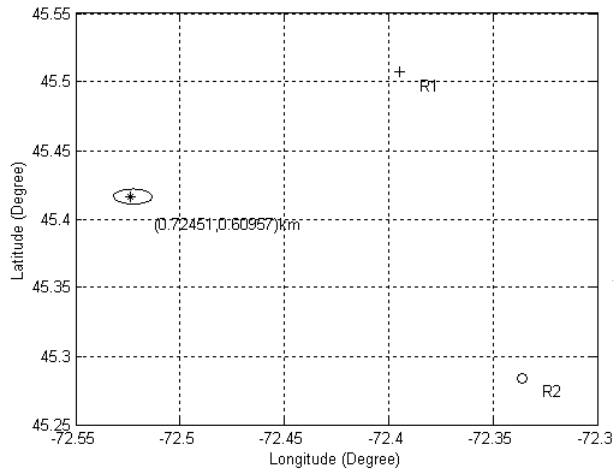


Fig. 6. Test1, WGS84, 1° SD, 99% CE, Avg_20snaps

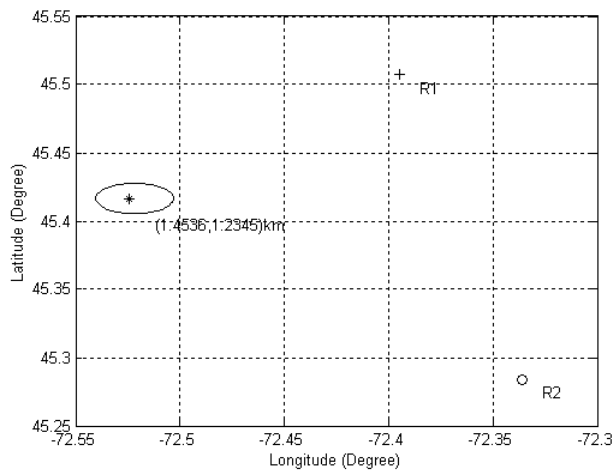


Fig. 7. Test1, Spherical, 2° SD, 99% CE, Avg_20snaps

Simulated Test2 Scenario: Mobile T1&T2 for a 2R fixing with 2° AOA SD and $P = 99\%$ CE.
 $AOA_{1,2_T1}(1,2) = (225^\circ, 228^\circ), (315^\circ, 318^\circ)$,
 $AOA_{1,2_T2}(1,2) = (235^\circ, 238^\circ), (325^\circ, 328^\circ)$. Among 20 snapshots, the results for the Spherical and WGS84 models are shown in Fig. 9 and Fig. 10, respectively. The related results are shown in TABLE I.

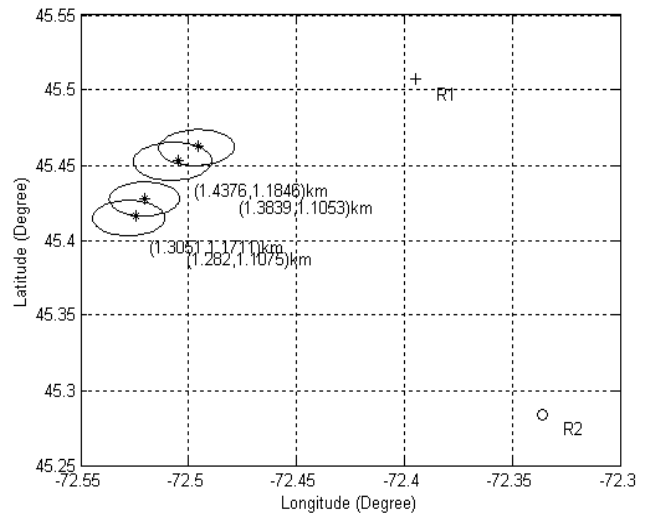


Fig. 9. Test2, Spherical, 2° SD, 99% CE, Avg_20snaps

Simulated Test3 Scenario: Mobile T1&T2 for a 3R fixing with 2° AOA SD and $P = 99\%$ CE.
 $AOA_{1,2,3_T1}(1,2) = (225^\circ, 228^\circ), (315^\circ, 318^\circ), (90^\circ, 93^\circ)$,
 $AOA_{1,2,3_T2}(1,2) = (235^\circ, 238^\circ), (325^\circ, 328^\circ), (80^\circ, 83^\circ)$.

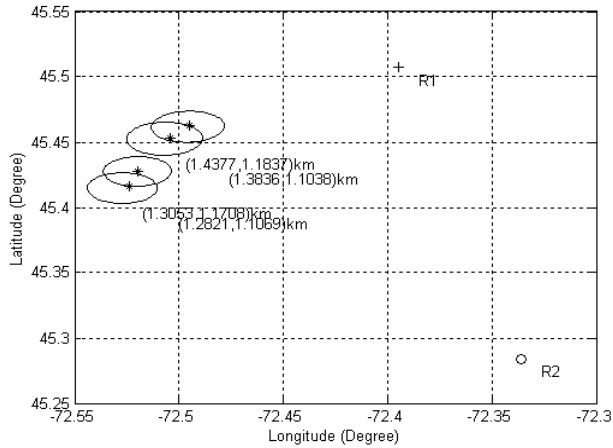


Fig. 10. Test2, WGS84, 2° SD, 99% CE, Avg_20snaps

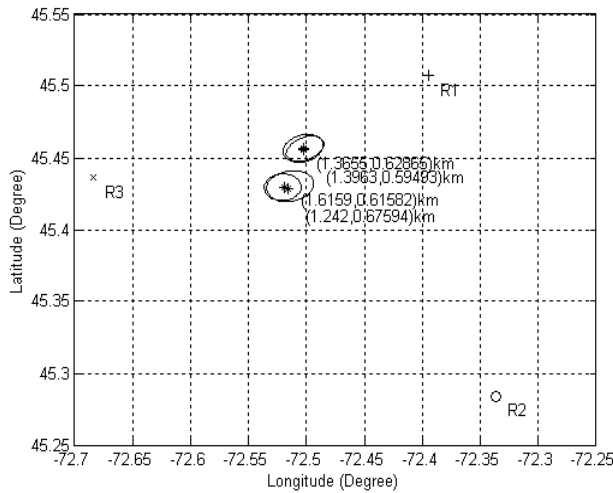


Fig. 11. Test3, Spherical, 2° SD, 99% CE, Avg_20snaps

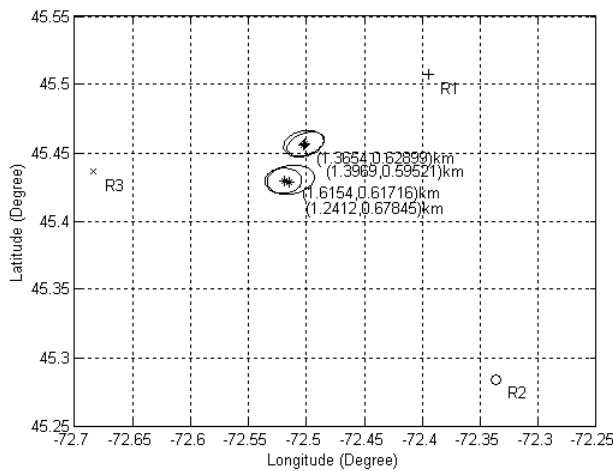


Fig. 12. Test3, WGS84, 2° SD, 99% CE, Avg_20snaps

Among 20 snapshots, the results for the Spherical and WGS84 models are shown in Fig. 11 and Fig. 12, respectively. The related results are shown in TABLE I.

From TABLE I Test1 part, one can see that the $(Er_AOAi_Tj, Vavg_Tj, RMSD_Tj)$ are independent of CEs (that is, 50% and 99% CEs have the same $(Er_AOAi_Tj, Vavg_Tj, RMSD_Tj)$).

However, the higher percentage the CE has, the larger (r_max, s_max) and AREACE_Tj are. Note that the capability to locate a transmitter properly relies on the accuracy of the area enclosed by the CE, which in turn, depends on the accuracy of $Vavg$ and (r_max, s_max) . Among the 2R and 3R fixings, the AOA SDs are involved in calculation of both $Vavg$ and (r_max, s_max) for the 3R fixing, while for the 2R fixing, the AOA SDs are only involved in calculation of (r_max, s_max) .

From TABLE I Test2&3 parts, the (Er_AOA1_Tj, Er_AOA2_Tj) in the 2R fixing are smaller than their counterparts in the 3R fixing. This may come from the involvement of the AOA SDs in (17), (18) and (19) to calculate $Vavg$ for the 3R fixing and the effect of the AOA SDs not being used to calculate $Vavg$ for the 2R fixing. Nevertheless, one can see that the Er_AOAi_Tjs are small (less than 2.25 SD of AOA SDs) in both the 2R and 3R fixings, which shows the accuracy of the two geodetic models in this study is significant. However, since the AOA SDs are not used to calculate $Vavg$ for the 2R fixing, with the extra information from the third receiver plus the AOA SDs, the accuracy of $Vavg$ should be higher for the 3R fixing. Also, the accuracy of (r_max, s_max) should be higher for the 3R fixing with the extra information from the third receiver, this can be seen from TABLE I that AREACE_Tjs of the CEs in the 2R cases are generally larger than their counterparts in the 3R cases.

The size of a CE at a certain percentage provides direct information of how confident a transmitter is located within that CE. That is, the larger the CE is, the higher the confidence is. At a certain confidence percentage, a smaller CE indicates a more accurate estimate of a transmitter's location. Thus, with higher accuracy of $Vavg$, (r_max, s_max) , and smaller AREACE, the 3R fixing can locate the transmitters better than the 2R fixing with the tradeoff that one more receiver is needed. Due to different calculations for V , the True_Tjs in the 2R cases have different values from their counterparts in the 3R cases. From the above discussion, one can see that the reason why the RMSD_Tjs in the 2R cases are not always larger than their counterparts in the 3R cases may be caused by the inaccuracy of True_Tjs in the 2R cases.

As per the Spherical and WGS84 models, their estimated results are close to each other in this study.

TABLE I. RESULTS FOR 20 SNAPSHOTS

	Spherical	WGS84
Simulated Test1 (I): AOA1=225, AOA2=315 dgs, 1-dg SD, 50% conf.		
Er_AOA1/2_T1(dg)	0.21141/ 0.24453	-0.21142/0.24459
True_T1(la_dg,lo_dg)	(45.4162, -72.5244)	(45.4162, -72.5238)
Vavg_T1(la_dg,lo_dg)	(45.4164, -72.5231)	(45.4165, -72.5226)
(r_max, s_max)_T1(km)	(0.28111, 0.23656)	(0.28108, 0.23649)
RMSD_T1(km)	0.38072	0.38077
AREACE_T1 (km ²)	0.20891	0.20883
Simulated Test1 (II): AOA1=225, AOA2=315 dgs, 1-dg SD, 99% conf.		
Er_AOA1/2_T1(dg)	0.21141/ 0.24453	-0.21142/0.24459
True_T1(la_dg,lo_dg)	(45.4162, -72.5244)	(45.4162, -72.5238)
Vavg_T1(la_dg,lo_dg)	(45.4164, -72.5231)	(45.4165, -72.5226)
(r_max, s_max)_T1(km)	(0.72459, 0.60974)	(0.72451, 0.60957)
RMSD_T1(km)	0.38072	0.38077
AREACE_T1 (km ²)	1.388	1.3874
Simulated Test1 (III): AOA1=225, AOA2=315 dgs, 2-dg SD, 99% conf.		
Er_AOA1/2_T1(dg)	0.43712/0.49647	-0.43715/0.49652
True_T1(la_dg,lo_dg)	(45.4162, -72.5244)	(45.4162, -72.5238)
Vavg_T1(la_dg,lo_dg)	(45.4166, -72.5218)	(45.4167, -72.5212)
(r_max, s_max)_T1(km)	(1.4536, 1.2345)	(1.4535, 1.2342)
RMSD_T1(km)	0.76158	0.76167
AREACE_T1 (km ²)	5.6374	5.6359
Simulated Test2: AOA1_T1(1,2)=225,228, AOA2_T1(1,2)=315,318, AOA1_T2(1,2)=235,238, AOA2_T2(1,2)=325,328 dgs, 2-dg SD, 99% conf.		
Er_AOA1_T1(1,2)(dg)	0.32178, -0.047916	0.32177, -0.047892
Er_AOA2_T1(1,2)(dg)	-0.80228, -0.040003	-0.80221, -0.039927
True_T1(1)(la_dg,lo_dg)	(45.4162, -72.5244)	(45.4162, -72.5238)
True_T1(2)(la_dg,lo_dg)	(45.4277, -72.5205)	(45.4278, -72.5199)
Vavg_T1(1)(la_dg,lo_dg)	(45.4148, -72.5277)	(45.4149, -72.5272)
Vavg_T1(2)(la_dg,lo_dg)	(45.4275, -72.5205)	(45.4276, -72.52)
(r_max, s_max)_T1(1)(km)	(1.3051, 1.1711)	(1.3053, 1.1708)
(r_max, s_max)_T1(2)(km)	(1.282, 1.1075)	(1.2821, 1.1069)
RMSD_T1(1,2)(km)	0.72998/ 0.94992	0.73003/ 0.72995
AREACE_T1(1,2) (km ²)	4.8017/ 4.4606	4.801/ 4.4584
Er_AOA1_T2(1,2)(dg)	0.41135, -0.47495	0.41132, -0.47493
Er_AOA2_T2(1,2)(dg)	-0.48043, -0.29088	-0.48038, -0.29083
True_T2(1)(la_dg,lo_dg)	(45.4531, -72.5048)	(45.4531, -72.5043)
True_T2(2)(la_dg,lo_dg)	(45.463, -72.4955)	(45.4631, -72.4951)
Vavg_T2(1)(la_dg,lo_dg)	(45.4526, -72.5074)	(45.4527, -72.5069)
Vavg_T2(2)(la_dg,lo_dg)	(45.4618, -72.4963)	(45.4619, -72.4958)
(r_max, s_max)_T2(1)(km)	(1.4376, 1.1846)	(1.4377, 1.1837)
(r_max, s_max)_T2(2)(km)	(1.3839, 1.1053)	(1.3836, 1.1038)
RMSD_T2(1,2)(km)	0.87361/ 0.78357	0.87379/ 0.87371
AREACE_T2(1,2) (km ²)	5.3501/ 4.8054	5.3463/ 4.798
Simulated Test3: AOA1_T1(1,2)=225,228, AOA2_T1(1,2)=315,318, AOA3_T1(1,2)=90,93, AOA1_T2(1,2)=235,238, AOA2_T2(1,2)=325,328, AOA3_T2(1,2)=80,83 dgs, 2-dg SD, 99% conf.		
Er_AOA1_T1(1,2)(dg)	2.4732, 0.68219	2.459, 0.6615
Er_AOA2_T1(1,2)(dg)	4.4999, 0.34127	4.4743, 0.3225
Er_AOA3_T1(1,2)(dg)	2.6763, 0.17662	2.6639, 0.15849
True_T1(1)(la_dg,lo_dg)	(45.4289, -72.5158)	(45.4288, -72.5153)
True_T1(2)(la_dg,lo_dg)	(45.4291, -72.5194)	(45.4291, -72.5189)
Vavg_T1(1)(la_dg,lo_dg)	(45.4303, -72.5141)	(45.4303, -72.5137)
Vavg_T1(2)(la_dg,lo_dg)	(45.4295, -72.5206)	(45.4295, -72.5201)
(r_max, s_max)_T1(1)(km)	(1.6159, 0.61582)	(1.6154, 0.61716)
(r_max, s_max)_T1(2)(km)	(1.242, 0.67594)	(1.2412, 0.67845)
RMSD_T1(1,2)(km)	1.4094/ 0.68348	0.87823/ 0.87822
AREACE_T1(1,2) (km ²)	3.1262/ 2.6375	3.132/ 2.6455
Er_AOA1_T2(1,2)(dg)	0.81012, -1.657	0.81611, -1.6443
Er_AOA2_T2(1,2)(dg)	1.0897, -2.1499	1.1006, -2.1406
Er_AOA3_T2(1,2)(dg)	0.89494, -2.2815	0.90839, -2.2694
True_T2(1)(la_dg,lo_dg)	(45.4556, -72.5026)	(45.4557, -72.5021)
True_T2(2)(la_dg,lo_dg)	(45.4569, -72.5022)	(45.457, -72.5017)
Vavg_T2(1)(la_dg,lo_dg)	(45.4564, -72.5013)	(45.4565, -72.5008)
Vavg_T2(2)(la_dg,lo_dg)	(45.4566, -72.503)	(45.4567, -72.5025)
(r_max, s_max)_T2(1)(km)	(1.3655, 0.62865)	(1.3654, 0.62899)
(r_max, s_max)_T2(2)(km)	(1.3963, 0.59493)	(1.3969, 0.59521)
RMSD_T2(1,2)(km)	0.81975/ 0.95306	0.90192/ 0.90193
AREACE_T2(1,2) (km ²)	2.6968/ 2.6097	2.6981/ 2.612

V. Conclusions

The paper presents two geodetic models using data from two or three receivers to track the locations of mobile transmitters. To apply the techniques, one first has to obtain the estimated AOAs and AOA SDs from two or three receivers to each transmitter using his own method. The histogram-based algorithms in [1] can be used to calculate the estimated AOAs and AOA SDs from a receiver to various transmitters. Once the estimated AOAs and AOA SDs from each receiver to the mobile transmitters are obtained, both the Spherical and WGS84 geodetic models can be used to process the estimated data for each receiver to track the mobile transmitters with a 2R or 3R fixing.

The results showed the effectiveness of using both of the geodetic models to track mobile transmitters with a 2R or 3R fixing. One can see that the accuracy of the algorithms is significant. The 3R fixing can locate the transmitters better than the 2R fixing, with the tradeoff being that one more receiver is needed. Results using the Spherical and WGS84 models are very similar.

In general, both of the geodetic models provide a simple and efficient way to track mobile transmitters. The approach is particularly applicable for receivers using fast scanning devices and where items such as AOAs and their instantaneous SDs from several channels are reported per second. In the near future, measured data for a 2R or 3R fixing with mobile transmitters will be used to test the capability of the algorithms in this study.

VI. References

- [1] M.-W. Tu and F. Patenaude, "Channel Usage Classification Using Histogram-Based Algorithms for Fast Wideband Scanners," Proceedings of the 6th Annual International Symposium on Advanced Radio Technologies, Boulder, Colorado, March 2004.
- [2] G. Strang and K. Borre, "Linear Algebra, Geodesy, and GPS," 1997 Wellesley-Cambridge Press.
- [3] J.P. Snyder, "Map Projections – A Working Manual," U.S. Geological Survey Professional Paper 1395, United States Government Printing Office, Washington: 1987.
- [4] R.G. Stansfield, "Statistical Theory of D.F. Fixing," J. Inst. Elec. Engrs., Vol. 94, part IIIA, 15, pp. 762-770, 1947.
- [5] P. Chahine, M. Dufour, E. Matt, J. Lodge, D. Paskovich and F. Patenaude, "Monitoring of the Radio-Frequency Spectrum with a Digital Analysis System: An Update," Proceedings of the 16th International Wroclaw Symposium on EMC, Poland, June 2002.
- [6] B. Grünbaum and G.C. Shepard, "Ceva, Menelaus, and the Area Principle," Math. Mag. 68, 254-268, 1995.